

# Horizon: Microfluidic platform for the production of therapeutic microbubbles and nanobubbles

Cite as: Rev. Sci. Instrum. **92**, 074105 (2021); <https://doi.org/10.1063/5.0040213>  
Submitted: 11 December 2020 • Accepted: 17 June 2021 • Published Online: 21 July 2021

 Radwa H. Abou-Saleh,  Fern J. Armistead,  Damien V. B. Batchelor, et al.




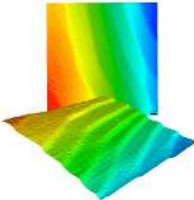



## ARTICLES YOU MAY BE INTERESTED IN

[Scaleable production of microbubbles using an ultrasound-modulated microfluidic device](#)  
The Journal of the Acoustical Society of America **150**, 1577 (2021); <https://doi.org/10.1121/10.0005911>

[Feedback-controlled microbubble generator producing one million monodisperse bubbles per second](#)  
Review of Scientific Instruments **92**, 035110 (2021); <https://doi.org/10.1063/5.0032140>

[Foam-free monodisperse lipid-coated ultrasound contrast agent synthesis by flow-focusing through multi-gas-component microbubble stabilization](#)  
Applied Physics Letters **116**, 173701 (2020); <https://doi.org/10.1063/5.0003722>

	<p>Nanopositioning Systems</p> 	<p>Modular Motion Control</p> 	<p>AFM and NSOM Instruments</p> 	<p>Single Molecule Microscopes</p> 
---	--	--	---	--



# Horizon: Microfluidic platform for the production of therapeutic microbubbles and nanobubbles

Cite as: *Rev. Sci. Instrum.* **92**, 074105 (2021); doi: [10.1063/5.0040213](https://doi.org/10.1063/5.0040213)

Submitted: 11 December 2020 • Accepted: 17 June 2021 •

Published Online: 21 July 2021



View Online



Export Citation



CrossMark

Radwa H. Abou-Saleh,<sup>1,2,3</sup>  Fern J. Armistead,<sup>1</sup>  Damien V. B. Batchelor,<sup>1</sup>  Benjamin R. G. Johnson,<sup>1,a)</sup>   
Sally A. Peyman,<sup>1,a)</sup>  and Stephen D. Evans<sup>1,a)</sup> 

## AFFILIATIONS

<sup>1</sup>Molecular and Nanoscale Physics Group, School of Physics and Astronomy, University of Leeds, Leeds LS2 9JT, United Kingdom

<sup>2</sup>Biophysics Group, Department of Physics, Faculty of Science, Mansoura University, Mansoura 35516, Egypt

<sup>3</sup>Nanoscience and Technology Program, Faculty of Advanced Basic Science, Galala University, Galala Plateau 43511, Egypt

<sup>a)</sup>Authors to whom correspondence should be addressed: [B.R.G.Johnson@leeds.ac.uk](mailto:B.R.G.Johnson@leeds.ac.uk), [S.Peyman@leeds.ac.uk](mailto:S.Peyman@leeds.ac.uk), and [S.D.Evans@leeds.ac.uk](mailto:S.D.Evans@leeds.ac.uk)

## ABSTRACT

Microbubbles (MBs) have a multitude of applications including as contrast agents in ultrasound imaging and as therapeutic drug delivery vehicles, with further scope for combining their diagnostic and therapeutic properties (known as theranostics). MBs used clinically are commonly made by mechanical agitation or sonication methods, which offer little control over population size and dispersity. Furthermore, clinically used MBs are yet to be used therapeutically and further research is needed to develop these theranostic agents. In this paper, we present our MB production instrument “Horizon,” which is a robust, portable, and user-friendly instrument, integrating the key components for producing MBs using microfluidic flow-focusing devices. In addition, we present the system design and specifications of Horizon and the optimized protocols that have so far been used to produce MBs with specific properties. These include MBs with tailored size and low dispersity (monodisperse); MBs with a diameter of  $\sim 2 \mu\text{m}$ , which are more disperse but also produced in higher concentration; nanobubbles with diameters of 100–600 nm; and therapeutic MBs with drug payloads for targeted delivery. Multiplexed chips were able to improve production rates up to 16-fold while maintaining production stability. This work shows that Horizon is a versatile instrument with potential for mass production and use across many research facilities, which could begin to bridge the gap between therapeutic MB research and clinical use.

© 2021 Author(s). All article content, except where otherwise noted, is licensed under a Creative Commons Attribution (CC BY) license (<http://creativecommons.org/licenses/by/4.0/>). <https://doi.org/10.1063/5.0040213>

## I. INTRODUCTION

Microbubbles (MBs) are widely used as contrast agents in ultrasound (US) imaging, where the air–liquid interface scatters and reflects US more effectively than tissue interfaces within the body.<sup>1</sup> Additionally, in the presence of US, MBs undergo volumetric oscillations driving them at or near to their resonance frequency that leads to considerable enhancement.<sup>2</sup> Another area of MB research involves their use as therapeutic delivery vehicles, such as for targeted delivery of chemotherapy drugs and delivery of DNA/siRNA vectors for gene therapy.<sup>3</sup> Combination of their therapeutic and diagnostic (i.e., theranostic) applications is also of interest.<sup>4</sup>

Traditionally, MBs are generated either by mechanical agitation or by sonication of a solution of lipids saturated with a low solubility gas, producing MBs 1–10  $\mu\text{m}$  in diameter.<sup>5</sup> The resonance frequency of MBs is inversely proportional to their size, and the frequency

bandwidth of typically used US transducers is narrow compared to the size distributions produced using these methods.<sup>6</sup> As such, these methods offer little control over MB size and dispersity, limiting its contrast enhancing abilities. Even so, commercial MBs are typically produced by mechanical agitation (e.g., SonoVue<sup>7</sup>) and used clinically as ultrasound contrast agents (UCAs). However, further research is needed before therapeutic or theranostic MBs become a viable treatment method for clinical use.

Microfluidics (MF) is widely utilized across multiple disciplines as the small required liquid volumes lead to reduced reaction times and minimal reagent consumption while lowering costs compared to larger batch technologies. Different groups have used microfluidics to produce MBs<sup>8–10</sup> using various MF geometries, such as T-junctions, flow-focusing (FF), and co-axial flow devices.<sup>11–16</sup> FF is the most commonly used geometry, consisting of a discontinuous gas phase being squeezed through a narrow orifice

(or “nozzle”) by a continuous liquid phase. The velocity gradient and resultant pressure drop results in gas phase “pinch-off” into the device outlet, producing MBs.<sup>10,17</sup> FF has demonstrated greater control over MB size compared to conventional methods through control of nozzle dimensions, gas pressure, and the liquid flow rate.<sup>17,18</sup>

Here, we present a robust, small footprint platform named “Horizon”, which utilizes FF microfluidic devices for MB production. Our platform is designed to be user-friendly and integrates key components for multi-application MB production, including high stability gas and liquid supplies, custom stage for microfluidic device integration that allows rapid switching between chips, an inverted microscope, and an additional port for the attachment of external cameras for high speed imaging. It offers good control over MB size and dispersity compared to conventional techniques and can also be used to produce specialized therapeutic microbubbles (thMBs).

Multiple chip-designs, substrate material [e.g., polymethylmethacrylate (PMMA) and polydimethylsiloxane (PDMS)], and geometries can be readily integrated in a “plug and play” manner, allowing MB populations to be tailored for size, dispersity, and concentration. FF devices are typically used to produce MB populations with a narrow size distribution, referred to as monodisperse MBs (MD-MBs). These offer improved clinical ultrasound response and tailoring of optimum size for application.<sup>18–20</sup> MF based MD-MB production techniques typically have a much lower production rate and final concentration of MBs ( $10^6$ – $10^8$  MBs/ml) compared to the mechanical agitation method ( $10^{10}$ – $10^{11}$  MBs/ml).<sup>21</sup> However, it has been shown that monodisperse samples can achieve the same contrast enhancement with tenfold lower concentration compared to mechanical agitation.<sup>22</sup> However, MBs with a therapeutic payload may require a higher concentration for effective delivery and treatment. Another factor to consider is the production rate, and commercial MBs are commonly supplied as a lyophilized lipid powder in a sealed vial with a low-solubility gas head space and can be activated by mechanical agitation in 45 s,<sup>23</sup> resulting in a polydisperse population. Comparatively, the production rate of recent MD-MBs has reached  $10^4$ – $10^6$  MBs/s<sup>6</sup> with 1 ml of sample produced in ~7 min also reported.<sup>24</sup>

Our previous work developed the microspray regime for MB production, which produces an average bubble diameter of ~2  $\mu\text{m}$  at concentrations of up to  $10^9$  MBs/ml.<sup>8,25</sup> Using Horizon, 1 ml of microspray MBs can be produced in ~3 min. In addition to MB production, this regime also produces nanobubbles (NBs) with diameters between 100 and 600 nm at concentrations up to  $10^{12}$  NBs/ml.<sup>26,27</sup> NBs have emerged as specialized candidates for extravascular drug delivery and imaging, showing increased tumor uptake and retention due to their smaller size compared to MBs.<sup>28–30</sup>

Our “Horizon” platform has also been utilized for therapeutic MB (thMB) production, achieved using a single operation of a microspray microfluidic device. This includes thMBs with a payload of drug-loaded liposomes for water soluble drugs<sup>31,32</sup> or lipid-oil-nanodroplets (LONDS) for hydrophobic drug delivery.<sup>33–35</sup> Therapeutic MBs have been successfully used to deliver chemotherapeutic drugs combined with an ultrasound trigger, showing improved delivery to colorectal cancer xenografts in murine models<sup>36</sup> as well as to microfluidic 3D spheroid models.<sup>37</sup> Additionally, it has been

shown that thMBs produced by Horizon can be freeze-dried and stored until required while retaining their drug-loading and structural integrity upon reconstitution.<sup>38</sup>

This paper presents the design and specifications of Horizon, which make it a robust and user-friendly system for the production of different micro- and nano-bubble samples. A key feature of Horizon is its portability and relatively small footprint compared to a non-integrated assembly of the same features such that the instrument can be easily re-located between different laboratories, research institutes, or potentially the clinic. We also describe the materials and methods required to use Horizon for reproducible MB applications. These include microspray regime MB production (including NB production), monodisperse MB production, and thMB production. The integrative nature of Horizon leaves scope for its use for other applications, for example, this could include adapting devices for production of monodisperse liquid droplets<sup>39</sup> and Giant Unilamellar Vesicles (GUVs).<sup>37</sup>

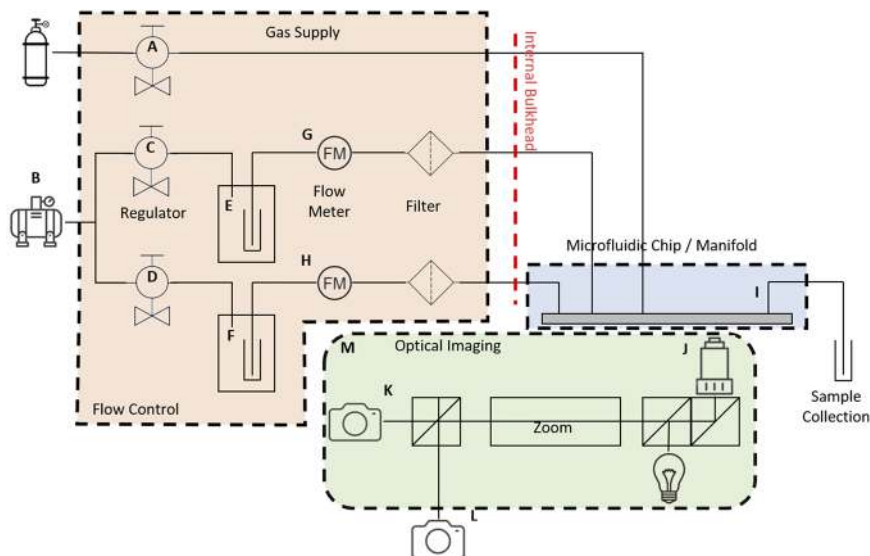
## II. SYSTEM DESIGN AND SPECIFICATIONS

The Horizon instrument is made up of four sections (fluid flow control, gas supply, manifold/microfluidic chip holder, and optical microscopy) that integrate to provide the overall instrument. A schematic of the internal components is shown in Fig. 1, showing gas supply components (orange), fluidic components (blue), and optical components (green). A photograph of the Horizon system is shown in Fig. 2(a).

Fluid flow is controlled using pressure-based Mitos P-pumps, Dolomite (Royston, UK). These pumps are pressured by compressed air (Fig. 1, A), fed into the instrument at 10 bars, which is then split inside Horizon, to provide supplies to both pressure control modules (Fig. 1, C and D). These controllers ensure a stable pressure is applied to each chamber (Fig. 1, E and F), which acts to displace liquid (containing bubble formulation and drug delivery vectors/targeting agents). The displaced fluid is collected through a metal needle that is immersed in the fluid [Fig. 2(b)], within the relevant chamber and passes through a flow sensor (Fig. 1, G and H) which measures the flow rate and a 0.45  $\mu\text{m}$  filter (Fig. 1, I) to remove any particulates present in solution. Each P-pump provides different ranges of liquid flow rates. Fluid flow rates in the range of 0.07–1000  $\mu\text{l}/\text{min}$  are typically possible using the Dolomite Flow Control Centre software [on a windows personal computer (PC)] and separate USB:RS232 connectors with a powered USB 3.0 hub.

Control of the gas used as the MB core [e.g., perfluorobutane ( $\text{C}_4\text{F}_{10}$ ), F2 Chemicals, Preston, UK] is through a further P-pump OEM module (Fig. 1, A). This acts by controlling the pressure rather than the flow of the gas but can provide a much greater degree of control than other pressure controllers. Control is through the Dolomite Flow Control Centre software to a precision of  $\pm 2$  mbar.

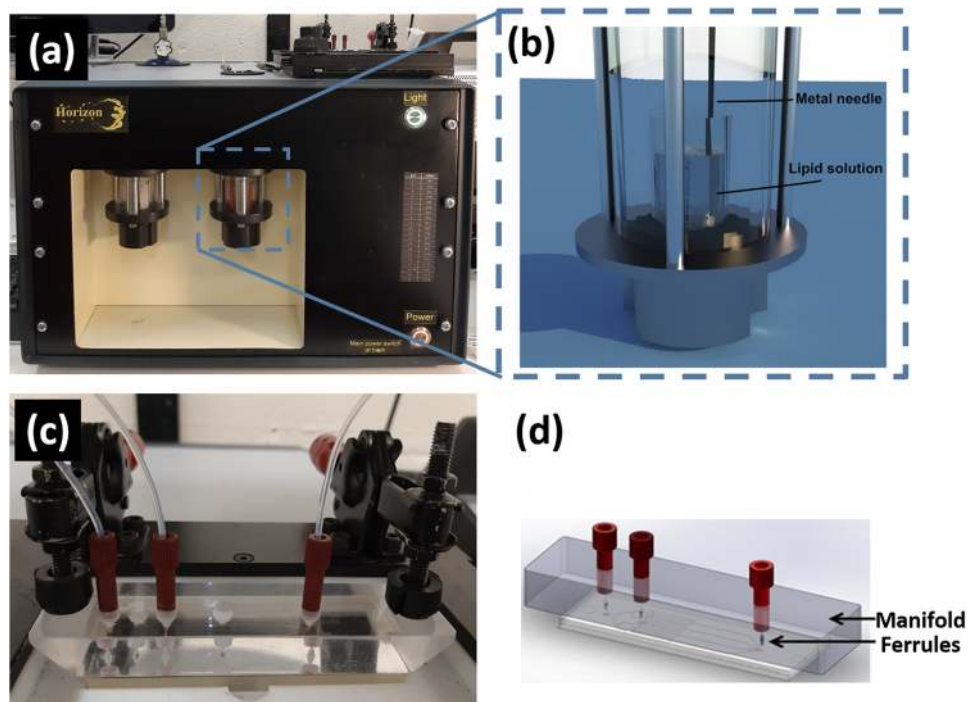
Optical viewing of the MB production region of the chip is possible via an integrated optical system (Opto, Daresbury, UK), which encompasses a high intensity LED based, coaxial Kohler illumination system and motorized focus with a 20 $\times$  objective in an inverted arrangement (Fig. 1, J). The reflected light is collected and passed through a variable motorized zoom module (7:1) and is then split between an internal c-mount camera (Fig. 1, K) (Meros, Dolomite,



**FIG. 1.** Schematic of the internal components of Horizon. A, C, and D: Dolomite (Royston, UK) P-pump OEM control module. E and F: Dolomite P-pump remote chamber. G and H: Dolomite MitoS flow rate sensor module (with choice of sensors from 70 nl/min to 1000  $\mu$ l/min). M: optical imaging components: Kohler coaxial illumination, motorized focus (with 20 $\times$  objective, J), motorized zoom (7:1), and 50:50 beam splitter for c-mount (internal camera, K) and f-mount (external high speed, L) (Opto UK Ltd., Daresbury, UK). K: Meros camera (Dolomite, Royston, UK).

Royston, UK) or an externally mounted f-mount for the attachment of high-speed camera systems (Fig. 1, L). The Dolomite Flow Control Centre allows for the simultaneous viewing of the camera and control of the P-pump modules—thus allowing the whole system to

be controlled through a single software interface. An internal bulkhead allows for the replacement of tubing with only minor disassembly and is separated from other internal components, e.g., electronics and optics.



**FIG. 2.** Horizon, the MF platform. (a) An image of the Horizon microfluidic platform. (b) Schematic of the vial holder that sits inside the P-pump chamber used to supply the liquid flow: the holder is made to fit different sizes of vials, with the metal needle that transmits the liquid to the chip. (c) The recess with a chip and the manifold with all the inlets and outlet tubing connections. (d) A 3D schematic diagram showing the assembly of the manifold on the chip for tight sealing.

The MF chips are mounted into a custom-built holder consisting of a recess into which the microchip sits [Figs. 2(c) and 2(d)]. A transparent polycarbonate manifold holds the polytetrafluoroethylene (PTFE) tubes (Supelco Analytical, USA) for liquid and gas lines and brings them into firm contact with the chip using a lever clamping arm to ensure a gas tight seal between the manifold and the chip [Fig. 2(c)].

A vial containing the lipid solution is introduced into the P-pump chamber, as shown in Fig. 2(b). The liquid flow rate and fluorocarbon gas pressure were adjusted according to the production regime and the type of MF chip used. MB production was carried out according to our previously described protocols<sup>8,25</sup> using either microspray chips or monodisperse chips. Dolomite Flow Control Centre software was used to simultaneously control the gas and liquid flow rates and visualize production using bright-field microscopy.

### III. MATERIALS AND METHODS

#### A. Materials

The lipids used for the data presented here were 1,2-dipalmitoyl-*sn*-glycero-3-phosphocholine (DPPC), 1,2-distearoyl-*sn*-glycero-3-phosphoethanolamine-N-[methoxy (polyethylene-glycol)-2000] (DSPE-PEG<sub>2000</sub>), and 1,2-distearoyl-*sn*-glycero-3-phosphoethanolamine-N-[biotinyl (polyethylene-glycol)-2000] (DSPE-B-PEG<sub>2000</sub>) and were purchased from Avanti Polar Lipids (Alabaster, AL, USA) and used without further purification. All lipids were received in the powder form and then dissolved in 50/50 chloroform/methanol.

#### B. Device fabrication

MS-MF chips were designed at the University of Leeds and produced by Epigem plc (Redcar, UK) in PMMA (polymethylmethacrylate) and SU-8.<sup>40</sup> To investigate the effect of changing microfluidic geometry on both MS and MD-MBs, devices were produced using PDMS to allow for rapid prototyping of devices. Detailed soft and photolithography methods can be found in S1.

#### C. Microbubble size and concentration measurements

Here, we used optical imaging to measure the size and concentration of microbubble populations. For MS-MBs, an aliquot collected from the middle of the homogeneous MB solution was diluted tenfold using 4 mg/ml NaCl to facilitate counting and sizing of MBs. For MD-MBs, no dilution was required. From this, 30  $\mu$ l was introduced in a 50  $\mu$ m height chamber on a glass slide. MBs were allowed to rise for  $\sim$ 1 min before acquiring images to ensure that they were all in the same focal plane. An inverted microscope (Nikon, Japan) was used to image MBs on a 60 $\times$  magnification objective. A CCD camera (DS-Fil 5Mega pixel, Nikon, Japan) was used to capture 20 images for each sample, from which the concentration and size distribution were obtained using a custom MATLAB (MathWorks, US) script utilizing the Image Analysis Toolbox.<sup>41</sup>

#### D. Nanobubble size and concentration measurements

The size and concentration of NB populations were obtained using Nanoparticle Tracking Analysis (NTA) (NanoSight NS300,

Malvern Panalytical, UK). Samples were illuminated with a 488 nm laser, and single particles were tracked using NTA software (version 3.3). Prior to measurement, samples were diluted 1:1000 in 4 mg/ml NaCl.

### IV. MICROFLUIDIC MICROSPRAY (MS) MICRO- AND NANO-BUBBLE PRODUCTION

#### A. Lipid preparation

The lipid composition for MS-MB formulation (DPPC+DSPE-PEG<sub>2000</sub>) was mixed at the molar ratio of 95:5 mol. % as described previously.<sup>29</sup> Briefly, the lipid mixture was dried under a steady stream of nitrogen gas, leaving a thin lipid film on the vial walls. This dried film was then suspended in a solution containing 4 mg/ml NaCl and 1% glycerol (Sigma-Aldrich, St. Louis, MO, USA) to a final lipid concentration of 2 mg/ml unless otherwise specified. This solution was vortexed for 1 min before being placed in an ultrasonic bath for 1 h. When lipids were fully suspended, 10  $\mu$ l of perfluorohexane (C<sub>6</sub>F<sub>14</sub>) (Sigma-Aldrich, St. Louis, MO, USA) was added per ml of solution to saturate the solution and vortexed well prior to introducing into Horizon for MF production. The addition of C<sub>6</sub>F<sub>14</sub> has previously shown to increase the stability of MBs produced in the microspray regime.<sup>42</sup>

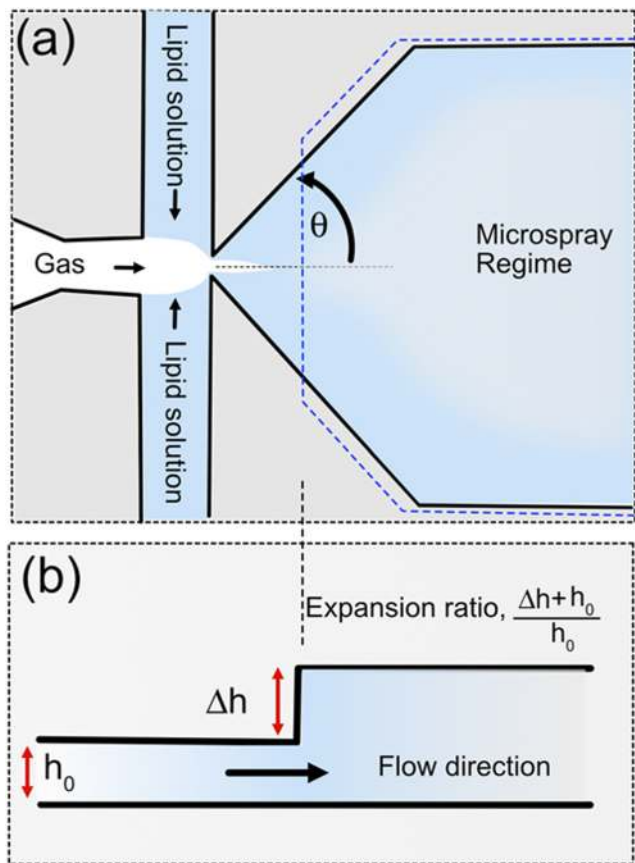
#### B. Chip design and optimization

The MF design has been described previously,<sup>8,25</sup> but briefly, it consists of a FF design with a central inlet channel for the gas and two opposing inlet channels for introduction of the liquid phase, a narrow orifice and a single outlet. In the microspray (MS) chip design (Fig. 3), the depth of the exit channel undergoes a sudden expansion (by 25  $\mu$ m), giving a total exit channel depth of 50  $\mu$ m [Fig. 3(b)]. This expansion causes a rapid pressure drop that results in the MBs being produced in the MS regime. To investigate the effect of changing microchannel geometry on the produced MB populations, the MF-spray devices were fabricated out of PDMS with various values of the expansion ratio, E, and outlet angle,  $\theta$ , as shown in Figs. 3(a) and 3(b) for the MS regime.

For increased production volumes, devices were multiplexed to have four [Fig. 4(a)], eight, or sixteen [Fig. 4(b)] FF nozzles per chip. This allowed the production of large volumes of MBs in less time, increasing the volumetric production rate from 1 ml in  $\sim$ 50 min using a single nozzle device to 1 ml in  $\sim$ 3 min using a  $\times$ 16 nozzle chip. These devices also have the advantage that if a single inlet becomes blocked, the remainder still function effectively.

#### C. Microspray microbubble and nanobubble production

Figure 5(a) shows an example of a typical batch of MS-MBs with a mean diameter of  $\sim$ 1.9  $\pm$  0.3  $\mu$ m and concentration of 10<sup>9</sup> MB/ml. Figure 5 shows that MS-MBs can be made using C<sub>4</sub>F<sub>10</sub>, SF<sub>6</sub>, and O<sub>2</sub> with no significant changes in concentration. Additionally, previous publications have used Horizon to make MS-MBs using C<sub>3</sub>F<sub>8</sub>.<sup>42</sup> These results show that these gases can be used to produce MS-MBs. However, the final gas core composition may be a mixture of the driving gas and air as Horizon drives the flow using compressed air ( $\sim$ 2–3 bars), which may satu-



**FIG. 3.** Schematic of the “microspray” chip. (a) Top view showing the 3D expansion region (blue dotted line) for high volume MB and NB production. (b) Side view showing the chip expansion region below the FF nozzle. The role of the outlet angle,  $\theta$ , and the expansion ratio  $(\Delta h + h_0)/h_0$  are described in the text.

rate the lipid solution and lead to air bubble nucleation post production. Regardless, these MBs have demonstrated size and concentration stability. In addition, previous studies using Horizon MS-MBs have shown that using the higher molecular weight gas  $C_4F_{10}$  compared to  $C_3F_8$  results in improved *in vivo* stability, suggesting that these gases were successfully encapsulated. Abou Saleh *et al.* (2020) also demonstrated  $O_2$  containing MS-MBs where the oxygen content was successfully measured using an  $O_2$  dipping probe.<sup>38</sup>

MS-MBs with a  $C_4F_{10}$  core made using Horizon were compared to five commercially available MBs (Table I).<sup>7,23,43–45</sup> MS-MBs produced by Horizon have a comparable mean diameter and *in vivo* lifetime to commercial UCAs while importantly containing fewer large MBs ( $>10 \mu m$ ) associated with increased risk of embolisms. Abou-Saleh *et al.* (2016) showed *in vivo* stability, where MBs demonstrated increased contrast enhancement compared to clinically approved MBs, and a time to half peak of  $\sim 12$  min.<sup>42</sup> In addition to MB production, the MS regime co-produced NBs as described by Peyman *et al.*<sup>26</sup> and Batchelor *et al.*,<sup>27</sup> which can be separated from larger MBs via buoyancy.

The effect of MF chip design on MB and NB production was investigated by varying the expansion ratio,  $E$ , and outlet angle,  $\theta$ . The expansion ratio,  $E$ , was defined to quantify the 3D expansion geometry and associated pressure drop while also accounting for small variances in  $h_0$  ( $<5 \mu m$ ) due to the photolithography process [Fig. 3(b)].

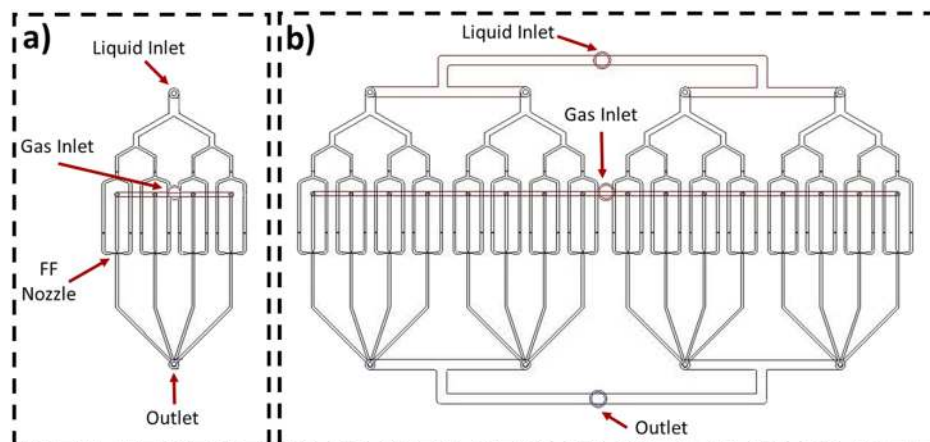
Figure 6 shows the concentration and diameter of MS-MBs as a function of expansion ratio and outlet angle ( $^\circ$ ), and these values were found using optical imaging as described in Sec. III C. Varying the depth of the expansion, with values of  $1 < E < 5$ , had little impact on MB concentration and diameter [Fig. 6(a)]. Furthermore, varying the outlet angle also showed little variation in MB size and concentration for  $\theta \geq 30^\circ$ . For values below this, the MB concentration decreases considerably from  $(9.6 \pm 2.8) \times 10^8 \text{ ml}^{-1}$  at  $\theta = 30^\circ$  to  $(1.03 \pm 0.22) \times 10^8 \text{ ml}^{-1}$  at  $\theta = 15^\circ$ , while the MB diameter did not vary significantly. Presumably, the reduction in concentration is due to a decrease in the pressure drop associated with smaller  $\theta$  values.

Figure 7 shows the concentration and diameter of the NB population produced by the microspray regime, as a function of expansion ratio and outlet angle ( $^\circ$ ). Due to the submicron size of NBs, these values were determined using Nanoparticle Tracking Analysis (NTA) as described in Sec. III C. It should be noted that NTA cannot distinguish between gas filled NBs,  $C_4F_{10}$  droplets, or lipid nanoparticles (i.e., liposomes) and as such determines the total particle concentration. However, previous work<sup>27</sup> documented the presence of sub-micron buoyant particles (e.g., NBs) produced by the microspray regime, while they have also demonstrated contrast enhancing properties.<sup>26</sup> Varying the expansion ratio and outlet angle had little effect on total nanoparticle populations (Fig. 7), similar to that as found with MBs. This may be expected as MBs and NBs are typically produced simultaneously.<sup>29</sup> In the future, it may be beneficial to repeat these experiments using alternate characterization techniques, which can distinguish between bubbles and non-bubbles (e.g., resonant mass measurement<sup>46</sup> or holographic NTA<sup>47</sup>). In summary, the MS regime is robust to even extreme changes in chip geometry, showing promise for scale up production of MBs and NBs.

#### D. Therapeutic MBs (thMBs)

The Horizon instrument is also capable of producing MBs with an attached drug payload (thMBs). In our previous works,<sup>32,36</sup> we utilized a biotin-streptavidin bridge for the attachment of drug-loaded liposomes, following a MF “one-pot” production method.<sup>8</sup> Here, biotinylated liposomes were incubated with NeutrAvidin (Life Technologies limited, UK) for 15 min prior to being added to a lipid solution containing a portion of biotinylated lipids (prepared for the MB production) and incubated for a further 15 min. Then, the whole mix is introduced into the Horizon for MF production of thMBs with liposomes as depicted in the schematic shown in Figs. 8(a) and 8(b).

Figure 9 shows reproducibility data that have been collected for bare MBs (not conjugated to liposomes) and the thMBs, showing consistent MB concentrations with and without conjugation [Fig. 9(a)]. A slight increase in diameter and an increase in the proportion of larger MBs ( $>10 \mu m$ ) were observed; however, these values are still consistent with clinically approved UCAs, as shown in Table I.



**FIG. 4.** Scaling up and multiplexing MF-spray chips. (a) A standard "microspray" chip design consisting of 4 FF nozzles in parallel, each supplied by the same liquid and gas inlet with a single outlet for sample collection. (b) An example of the ability to increase the production rate by multiplexing the chip design, consisting of 16 parallel FF nozzles.

## V. MICROFLUIDIC MONODISPERSE MB PRODUCTION

### A. Lipid preparation

For the production of MD-MBs, the same lipid formulation of DPPC and DSPE-PEG<sub>2000</sub> was prepared at 4 mg/ml in a solution of MilliQ with 4 mg/ml of sodium chloride (NaCl). The initial resuspension of the dried lipid film involved heating in a dry bath to 45 °C (above the 41.3 °C transition temperature of DPPC) for ~15 min followed by ~1 min vortexing, until the lipid film was resuspended into a cloudy solution. This solution was then tip sonicated for 45 min, where the subsequent solution was clear. Dynamic light scattering (Zetasizer Nano ZS, Malvern Panalytical, UK) was used to confirm that the final lipid solution contained small liposomes ~90 nm (S2).

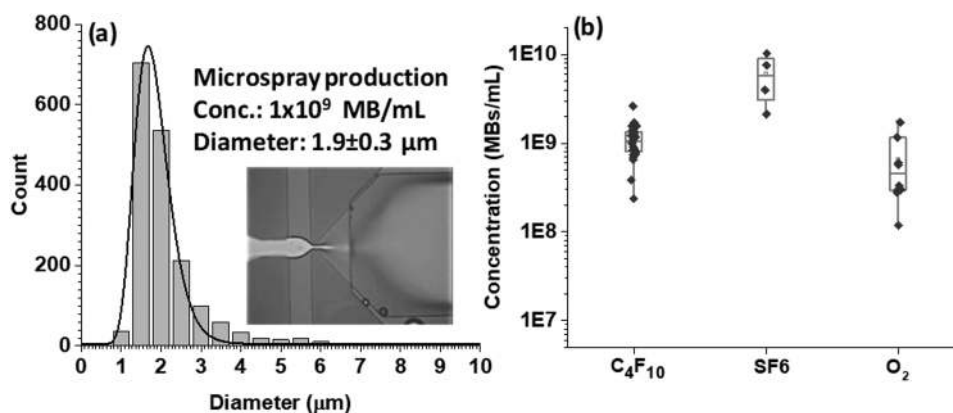
MD-MB production is highly sensitive to fluctuations in liquid flow rate, and the Horizon system software (Dolomite Flow Control Centre) automatically logs details of the gas and liquid flow rates over time during experiments such that the target flow rate can be compared to the actual flow rates and fluctuations can be quantified. It was found that using a lipid solution prepared via bath sonication

(Sec. III) led to large fluctuations in flow rate. As such, lipids were tip sonicated following the described method.

Fluctuations of the liquid flow rate sensor were measured for various solutions (S3) over >2 min and were quantified using the relative standard deviation (RSD), defined as the ratio of the standard deviation to the mean. MilliQ filtered through a 200 nm filter had RSD < 1%. Lipid solution prepared using a sonic bath had RSD = 15% fluctuation and improved to RSD = 5% fluctuation when filtered through a 200 nm filter. Tip sonication and filtering of lipids resulted in RSD < 1%, comparable to filtered MilliQ. Thus, tip sonication prepared lipids were found to be optimal for MD-MBs production, which is in alignment with lipid preparation methods by other groups who produce MD-MBs.<sup>6,13,48</sup> As MS-MBs are less susceptible to fluctuations, a tip sonicator can be used but is not required for production. Thus, an ultrasonic bath can also be used for their production.

### B. High speed microscopy

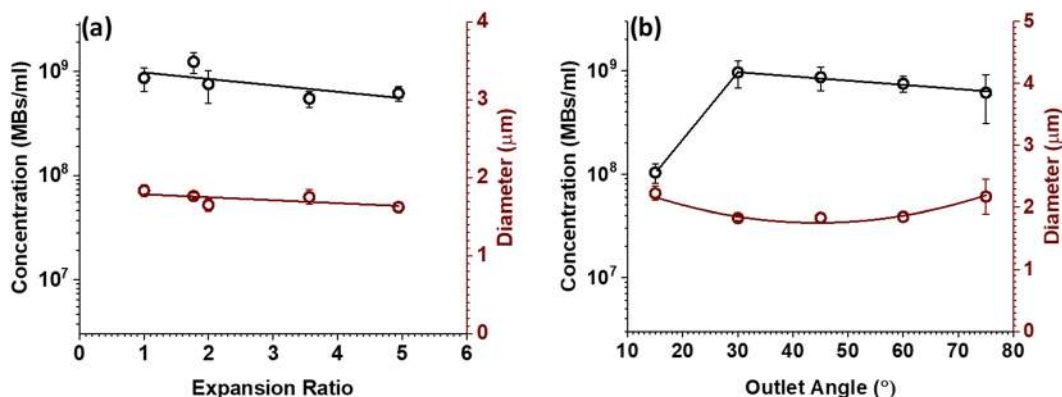
For MD-MB production, high speed microscopy (Shimadzu HPV-X, Japan) was used to observe on-chip bubble formation.



**FIG. 5.** (a) MB size distribution, with the inset showing the MS production regime. (b) Concentration of MBs produced with different gas cores: perfluorobutane (C<sub>4</sub>F<sub>10</sub>), sulfur hexafluoride (SF<sub>6</sub>), and oxygen (O<sub>2</sub>).

**TABLE I.** Comparing in-house Horizon MBs with commercially available MBs.

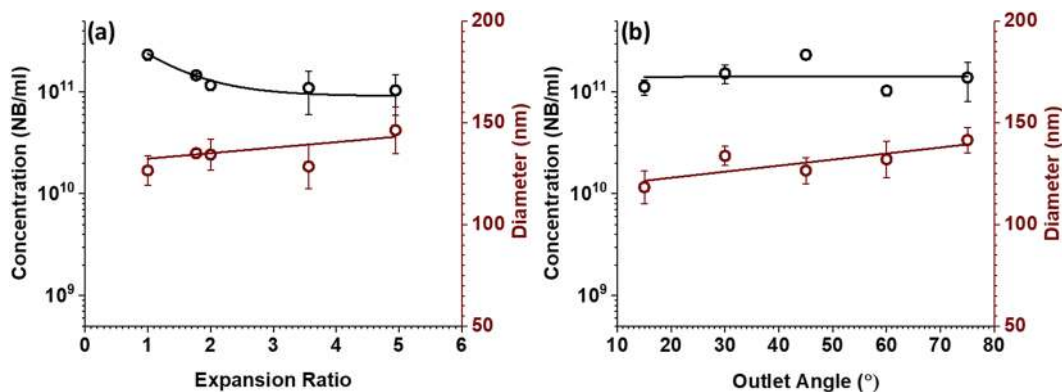
MB name	Shell	Gas	Conc.	Lifetime <i>in vivo</i> (min)	Diameter ( $\mu\text{m}$ )	%<10 ( $\mu\text{m}$ )	%<11 ( $\mu\text{m}$ )	Max diameter ( $\mu\text{m}$ )
Definity (Lantheus Medical Imaging, Inc., and Bristol-Mayers Medical Imaging)	Lipids	$\text{C}_3\text{F}_8$	$1.2 \times 10^{10}$	3.4	1.1–3.3	98		20
SonoVue (Bracco)	Lipids	$\text{SF}_6$	$2 \times 10^8$	12	2.5		99	
MicroMarker (Bracco)	Lipids	$\text{C}_4\text{F}_{10} + \text{N}_2$	$2 \times 10^9$	15–20	2.3–2.9			
Optison (Molecular biosystems Mallinckrodt Inc. and GE Healthcare)	Albumin	$\text{C}_3\text{F}_8$	$5\text{--}8 \times 10^8$	3	3–4.5		95	32
Echovist-200 (Berlex Canada)	Galactose	air			2	99		
Horizon	Lipids	$\text{C}_4\text{F}_{10} + \text{C}_6\text{F}_{14}$	$1 \times 10^9$	12	2		99.2	17.5

**FIG. 6.** Effect of varying chip parameters on the MB size (red line) and concentration (black line). (a) Varying expansion ratio,  $(\Delta h + h_0)/h_0$  (and  $h_0 \sim 25 \mu\text{m}$ ). (b) Changing outlet angle. The data for each point represent the averages from at least three independent sample preparations, and error bars denote the standard error.

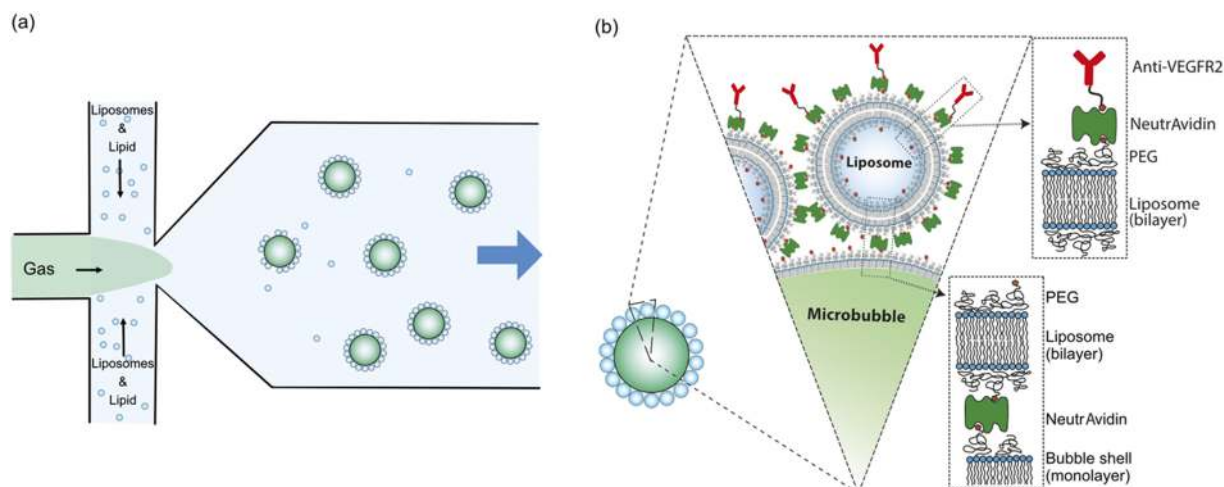
The camera was used at typical frame rates of 200–500 K fps with a triggered external light to achieve sub-microsecond exposure times. During MD-MB production, the high-speed videos were viewed in near real-time to ensure the production was monodisperse and stable over time. Figure 10 (Multimedia View) shows a typical monodisperse production.

### C. Chip design and optimization

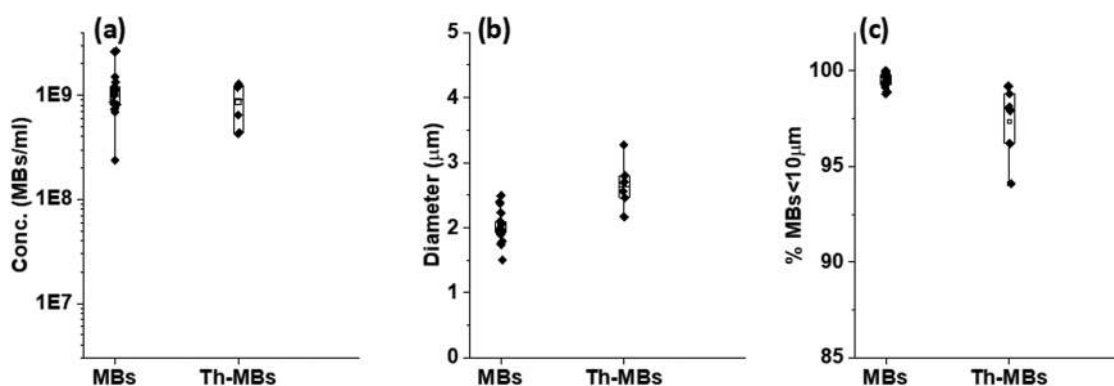
Figure 10(a) shows the FF MF chip design for producing MD-MBs using Horizon. The FF design results in pinch-off at the nozzle, resulting in a single stream of MD-MB with a controlled and narrow size distribution.

**FIG. 7.** Varying chip parameters on the produced NB size (red line) and concentration (black line). (a) Changing expansion ratio. (b) Changing outlet angle. The data for each point represent the averages from at least three independent sample preparations, and error bars denote the standard error.





**FIG. 8.** Microfluidic chip production of drug loaded MBs. (a) One-pot production for MBs +liposomes using the same chip design for MB production. (b) Schematic of MBs with drug loaded liposomes attached to the MB shell (not drawn to scale). The antibody targeting agent is added off chip in this example.<sup>36</sup> Reproduced with permission from Ingram *et al.*, *Theranostics* **10**(24), 10973–10992 (2020). Copyright 2020, Ivyspring International Publisher.



**FIG. 9.** MBs and thMBs produced with Horizon. (a) Concentration of produced samples. (b) Modal diameter of the produced population. (c) Percentage of MBs smaller than 10  $\mu\text{m}$  in diameter.

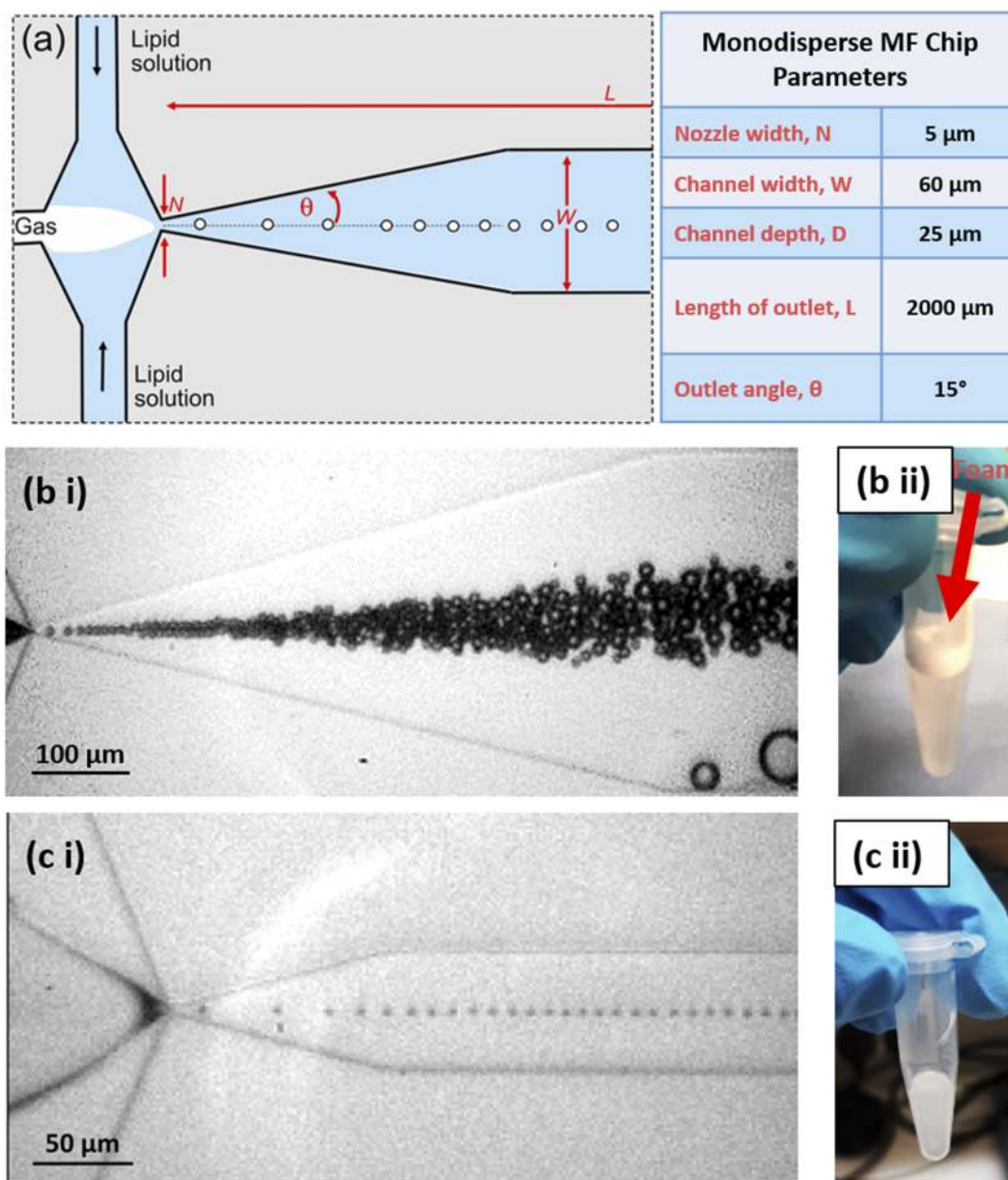
For MD-MBs, devices were designed and fabricated from PDMS using standard lithography techniques (S1). The schematic in Fig. 10(a) shows the basic geometry and main device dimensions. The optimum chip design had a continuous depth of 25  $\mu\text{m}$ ; a nominal nozzle width,  $N$ , of 5  $\mu\text{m}$ ; an outlet angle,  $\theta$ , of 15°; and an outlet width,  $W$ , of 60  $\mu\text{m}$ .

Changes in chip dimensions were made to maximize sample monodispersity and concentration. Figure 10(b) shows an example where the outlet angle is  $\theta = 15^\circ$  and the outlet width is 360  $\mu\text{m}$ . Attempts to produce MD-MBs using these devices proved unsuccessful across a wide range of flow conditions. Figure 10(b-i) shows that as the outlet widens, the MD-MBs slow down during their flow post-production, leading to bubble collisions and coalescence shortly after production. Figure 10(b-ii) shows an example of such MBs post production. A large foam layer can be seen at the surface, forming quickly after production and even after gentle mixing. Samples contained only large bubbles ( $\gg 10 \mu\text{m}$ ) with negligible

MBs remaining, hence the quick separation of the sample. This is indicative of on-chip MB coalescence and poor stability.

Foam has also been observed due to Ostwald ripening, which occurs due to gas exchange between newly produced MBs, resulting in large bubbles  $>100 \mu\text{m}$  as well as the MD-MB population, and is amplified in highly concentrated samples.<sup>49</sup> Segers *et al.* (2020) used a mixture of low and high aqueous solubility gas to prevent this effect, forming foam-free MD-MB samples at high production rates ( $4 \times 10^5$  MBs/s).<sup>24</sup> These studies required using two gas canisters simultaneously, enclosing the system inside an oven at 55 °C, a water bath to hold the microfluidic device, and a cooling mechanism around the outlet to reduce MB temperature post production.

Comparatively, Fig. 10 shows that Horizon can be utilized to produce MD-MBs at room temperature simply by changing the microfluidic device geometry to prevent on-chip coalescence. Figure 10(c) shows production using the optimum geometry/conditions for producing MD-MBs for a comparable production



**FIG. 10.** Schematic of the chip design used for MD-MBs with the main chip dimensions summarized in the table. (b-i) An example of unoptimized MB production from a PDMS device with an outlet angle,  $\theta$ , of  $15^\circ$  and an outlet width,  $W$ , of  $360\ \mu\text{m}$ . The gas pressure was 575 mbar, and the liquid flow rate was  $28\ \mu\text{l}/\text{min}$ . The wide channel after the nozzle and the high production rate of MD-MBs result in on-chip coalescence and polydispersity with an inset image (b-ii) of the collected sample in the Eppendorf. Here, a foam forms, containing large coalesced bubbles. (c-i) An example MB production from a PDMS device with the dimensions shown in the table. The gas pressure was 530 mbar, and the liquid flow rate was  $36\ \mu\text{l}/\text{min}$ . This design resulted in a stable MD production with no coalescence, with an inset image (c-ii) of the collected sample in the Eppendorf. Multimedia view: <https://doi.org/10.1063/5.0040213.1>

rate to Fig. 10(b). This design shows no MB coalescence on-chip, and Fig. 10(c-ii) shows MBs collected after production using this device. In these cases, the sample looks cloudy after gentle mixing and no foam layer containing large bubbles is observed, which suggests that the MBs are stable. Studies have shown that on-chip coalescence can

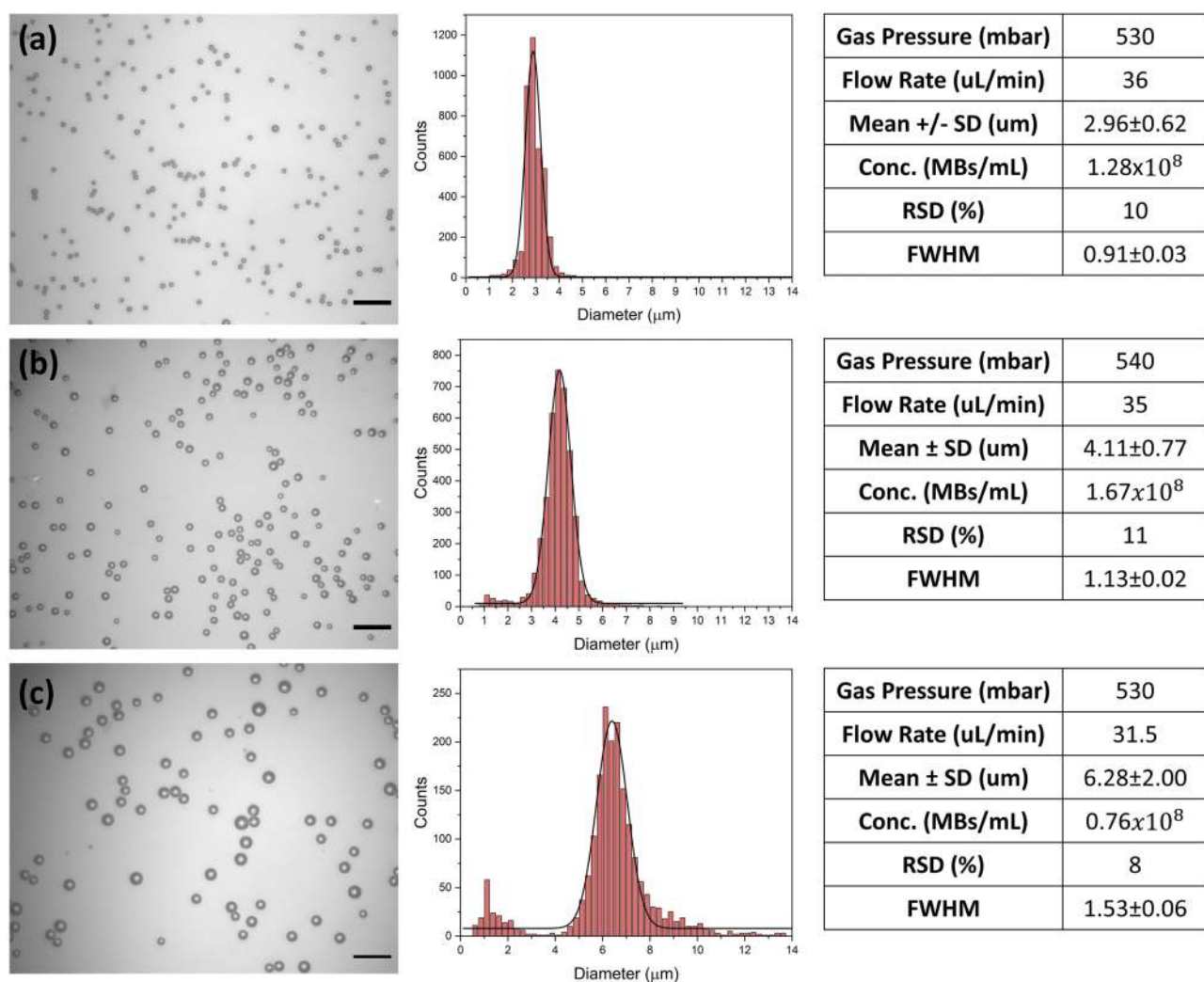
also be prevented using higher lipid concentrations ( $10\ \text{mg}/\text{ml}$ )<sup>6</sup> or by heating to higher temperatures ( $>50^\circ\text{C}$ ) and then quickly cooling back to room temperature post production.<sup>20</sup>

MD-MBs were characterized off-chip using optical microscopy as described in Sec. III C,<sup>41</sup> and monodispersity was classified using

the relative standard deviation (RSD), which was found by fitting Gaussian functions to the size distribution histograms. The standard deviation of the fit was divided by the peak center to find the RSD. MD-MBs also demonstrated stability over  $\sim 1$  day when stored at  $4^\circ\text{C}$  (S4) and were produced at comparable production rates to the recent literature (S5),<sup>6</sup> making it ideal for those without specialist equipment. Future iterations of the instrument could include heating elements and additional pumps for further optimization of MB production.

Figure 11 shows three examples of MD-MB off-chip analysis including a bright-field image, histogram of MB diameters, and a table summarizing the average size, concentration, and RSD of the MBs. Across the three datasets, the concentrations ranged between  $(0.76\text{--}1.67) \times 10^8$  MBs/ml and RSD between 8% and 11%.

Figure 11(a) has a mean MB diameter ( $\pm\text{SD}$ ) of  $2.9 \pm 0.6 \mu\text{m}$ , Fig. 11(b) has a mean MB diameter of  $4.1 \pm 0.8 \mu\text{m}$ , and Fig. 11(c) has a mean MB diameter of  $6.3 \pm 2.0 \mu\text{m}$ . The ratio of the liquid flow rate to the gas pressure ratio is known to affect MD-MB production rates and size.<sup>7</sup> In these examples, the gas pressures are 530–540 mbar and MB size decreased as the flow rate was increased between 31.5 and 36.0  $\mu\text{l}/\text{min}$ . These results show that the Horizon system can be used to produce MBs that are highly monodisperse, and the gas pressure and liquid flow rates can be tuned to achieve a range of MB diameters. S4 shows the average diameter and concentration of an MD-MB population as a function of time. This shows that MD-MBs produced using Horizon are stable over  $\sim 20$  h after production, showing a negligible change in dispersity and with  $\sim 70\%$  of the original concentration of MBs remaining.



**FIG. 11.** Three MD-MB samples (a)–(c) produced using the Horizon system to achieve different mean MB sizes. The MBs were imaged optically off-chip after production, and examples are shown with  $20 \mu\text{m}$  scale bars. Images were used to size the MBs, and the diameters were plotted as histograms fitted with Gaussian functions (black line). The tables summarize the mean, standard deviation, concentration, RSD, and FWHM of samples (a)–(c).

High-speed microscopy videos can also be used to calculate the on-chip MB production time and to estimate the expected concentration and diameters of collected MD-MB samples. S5 includes a description of how this type of analysis can be done and shows an example dataset using videos taken while the sample shown in Fig. 11(c) was collected. Comparing the measured diameters, concentrations, and dispersity both on- and off-chip can help elucidate sample stability and dynamics associated with bubble formation.

## VI. CONCLUSION

This paper describes the design of the portable, integrated, Horizon microfluidic platform to produce lipid coated MBs for application as contrast agents and drug delivery systems. Using the MF-spray regime, MBs can be produced at high volume and high concentration ( $10^9$  MB/ml) and with population distributions similar to those used as ultrasound contrast agents in clinics today. The MF spray regime also produces high concentrations of NBs that can be separated from the MB population, with future applications for high frequency contrast imaging and extravascular drug delivery.<sup>26,27,30,50</sup> By simply replacing the MF chip, the platform can produce monodisperse MB populations of controlled size, with potential benefits for both diagnosis and therapy. As a fully integrated system combining fluid and gas flow control and microscopy, the Horizon system could also be adapted for many other microfluidic applications. This portable, easy to use platform shows excellent production stability and robustness between different samples and different users,<sup>8</sup> and as such, the Horizon instrument can provide a variety of MB and NB formulations for use in contrast US and drug delivery studies.

## SUPPLEMENTARY MATERIAL

See the [supplementary material](#) for S1—production method of PDMS microfluidic devices; S2—DLS population distribution of liposomes used for monodisperse bubble production; S3—liquid flow rate sensor data logs for unfiltered MS-lipids, filtered MS-lipids, filtered MD-lipids, and MilliQ; S4—monodisperse microbubble concentration and size stability over 24 h; and S5—analysis of high-speed videos showing production of monodisperse microbubbles.

## AUTHORS' CONTRIBUTIONS

R.H.A., F.J.A., and D.V.B.B. contributed equally to experimental planning, data acquisition and analysis, and manuscript preparation. B.R.G., S.A.P., and S.D.E. contributed to the initial conceptualization and manuscript preparation. B.R.G. designed and constructed the Horizon instrument. S.A.P. and S.D.E. contributed to experimental planning and supervision.

## ACKNOWLEDGMENTS

The authors would like to acknowledge EPSRC for funding (Grant Nos. EP/I000623 and EP/K023845) and thank the Microbubble Consortium (<http://www.microbubbles.leeds.ac.uk/>) at the University of Leeds for useful discussions. S.D.E. was supported by the National Institute for Health Research infrastructure at Leeds. The views expressed are those of the author(s) and not

necessarily those of the National Health Service, the National Institute for Health Research, or the Department of Health. D.V.B.B. thanks K. de Silva for support through the provision of an Alumni PhD scholarship. We would like to thank the whole Mechanical and Electrical workshop teams in the School of Physics and Astronomy for their continued support and skills throughout the entirety of their work.

## DATA AVAILABILITY

The data that support the findings of this study are openly available in the University of Leeds data repository at <https://doi.org/10.5518/973>.

## REFERENCES

- 1 S. B. Murthi, M. Ferguson, and A. C. Sisley, *Diagnostic Ultrasound: Physics and Equipment* (Cambridge University Press, 2010).
- 2 J. R. Lindner, "Microbubbles in medical imaging: Current applications and future directions," *Nat. Rev. Drug Discovery* **3**(6), 527–532 (2004).
- 3 R. Browning and E. Stride, "Microbubble-mediated delivery for cancer therapy," *Fluids* **3**(4), 74 (2018).
- 4 S. R. Sirsi and M. A. Borden, "State-of-the-art materials for ultrasound-triggered drug delivery," *Adv. Drug Delivery Rev.* **72**, 3–14 (2014).
- 5 V. Daeichin *et al.*, "Microbubble composition and preparation for imaging: *In vitro* and *in vivo* evaluation," *IEEE Trans. Ultrason., Ferroelectr., Freq. Control* **64**(3), 555–567 (2017).
- 6 T. Segers, L. De Rond, N. De Jong, M. Borden, and M. Versluis, "Stability of monodisperse phospholipid-coated microbubbles formed by flow-focusing at high production rates," *Langmuir* **32**(16), 3937 (2016).
- 7 SonoVue, Summary of Product Characteristics, European Medicines Agency.
- 8 S. A. Peyman *et al.*, "Expanding 3D geometry for enhanced on-chip microbubble production and single step formation of liposome modified microbubbles," *Lab Chip* **12**(21), 4544 (2012).
- 9 M. Hashimoto and G. M. Whitesides, "Formation of bubbles in a multisection flow-focusing junction," *Small* **6**(9), 1051–1059 (2010).
- 10 P. Garstecki, M. J. Fuerstman, H. A. Stone, and G. M. Whitesides, "Formation of droplets and bubbles in a microfluidic T-junction—Scaling and mechanism of break-up," *Lab Chip* **6**(3), 437 (2006).
- 11 P. Garstecki, M. J. Fuerstman, M. A. Fischbach, S. K. Sia, and G. M. Whitesides, "Mixing with bubbles: A practical technology for use with portable microfluidic devices," *Lab Chip* **6**(2), 207–212 (2006).
- 12 E. Stride and M. Edirisinghe, "Novel preparation techniques for controlling microbubble uniformity: A comparison," *Med. Biol. Eng. Comput.* **47**(8), 883–892 (2009).
- 13 K. P. Pancholi, U. Farook, R. Moaleji, E. Stride, and M. J. Edirisinghe, "Novel methods for preparing phospholipid coated microbubbles," *Eur. Biophys. J.* **37**(4), 515–520 (2008).
- 14 K. Pancholi, E. Stride, and M. Edirisinghe, "Dynamics of bubble formation in highly viscous liquids," *Langmuir* **24**(8), 4388–4393 (2008).
- 15 E. Castro-Hernández, W. van Hove, D. Lohse, and J. M. Gordillo, "Microbubble generation in a co-flow device operated in a new regime," *Lab Chip* **11**(12), 2023–2029 (2011).
- 16 E. Talu, M. M. Lozano, R. L. Powell, P. A. Dayton, and M. L. Longo, "Long-term stability by lipid coating monodisperse microbubbles formed by a flow-focusing device," *Langmuir* **22**(23), 9487–9490 (2006).
- 17 P. Garstecki, I. Gitlin, W. Diluzio, G. M. Whitesides, E. Kumacheva, and H. A. Stone, "Formation of monodisperse bubbles in a microfluidic flow-focusing device," *Appl. Phys. Lett.* **85**(13), 2649–2651 (2004).
- 18 M. Seo, I. Gorelikov, R. Williams, and N. Matsuura, "Microfluidic assembly of monodisperse, nanoparticle-incorporated perfluorocarbon microbubbles for medical imaging and therapy," *Langmuir* **26**(17), 13855–13860 (2010).

- <sup>19</sup>K. Hettiarachchi, E. Talu, M. L. Longo, P. A. Dayton, and A. P. Lee, "On-chip generation of microbubbles as a practical technology for manufacturing contrast agents for ultrasonic imaging," *Lab Chip* **7**(4), 463–468 (2007).
- <sup>20</sup>T. Segers, A. Lassus, P. Bussat, E. Gaud, and P. Frinking, "Improved coalescence stability of monodisperse phospholipid-coated microbubbles formed by flow-focusing at elevated temperatures," *Lab Chip* **19**(1), 158–167 (2019).
- <sup>21</sup>C. Jiang *et al.*, "Microfluidic-assisted formation of multifunctional monodisperse microbubbles for diagnostics and therapeutics," *Micronano Lett.* **6**(6), 417–421 (2011).
- <sup>22</sup>A. Helbert, E. Gaud, T. Segers, C. Botteron, P. Frinking, and V. Jeannot, "Monodisperse versus polydisperse ultrasound contrast agents: *In vivo* sensitivity and safety in rat and pig," *Ultrasound Med. Biol.* **46**(12), 3339–3352 (2020).
- <sup>23</sup>DEFINITY (Perflutren Lipid Microsphere) Injectable Suspension, for intravenous use, Lantheus Medical Imaging.
- <sup>24</sup>T. Segers, E. Gaud, G. Casqueiro, A. Lassus, M. Versluis, and P. Frinking, "Foam-free monodisperse lipid-coated ultrasound contrast agent synthesis by flow-focusing through multi-gas-component microbubble stabilization," *Appl. Phys. Lett.* **116**(17), 173701 (2020).
- <sup>25</sup>S. A. Peyman, R. H. Abou-Saleh, and S. D. Evans, "Microbubbles for therapeutic delivery," *Ther. Delivery* **4**(5), 539–542 (2013).
- <sup>26</sup>S. A. Peyman *et al.*, "On-chip preparation of nanoscale contrast agents towards high-resolution ultrasound imaging," *Lab Chip* **16**(4), 679–687 (2016).
- <sup>27</sup>D. V. B. Batchelor, R. H. Abou-saleh, L. Coletta, J. R. McLaughlan, S. A. Peyman, and S. D. Evans, "Nested-nanobubbles for ultrasound triggered drug release," *ACS Appl. Mater. Interfaces* **12**, 29085 (2020).
- <sup>28</sup>C. Pellow, E. C. Abenojar, A. A. Exner, G. Zheng, and D. E. Goertz, "Concurrent visual and acoustic tracking of passive and active delivery of nanobubbles to tumors," *Theranostics* **10**(25), 11690–11706 (2020).
- <sup>29</sup>H. Wu, E. C. Abenojar, R. Perera, A. C. De Leon, T. An, and A. A. Exner, "Time-intensity-curve analysis and tumor extravasation of nanobubble ultrasound contrast agents," *Ultrasound Med. Biol.* **45**(9), 2502–2514 (2019).
- <sup>30</sup>D. V. B. Batchelor *et al.*, "Nanobubbles for therapeutic delivery: Production, stability and current prospects," *Curr. Opin. Colloid Interface Sci.* **54**, 101456 (2021).
- <sup>31</sup>J. R. McLaughlan, S. Harput, R. H. Abou-Saleh, S. A. Peyman, S. Evans, and S. Freear, "Characterisation of liposome-loaded microbubble populations for subharmonic imaging," *Ultrasound Med. Biol.* **43**(1), 346–356 (2017).
- <sup>32</sup>J. McLaughlan *et al.*, "High-frequency subharmonic imaging of liposome-loaded microbubbles," in *IEEE International Ultrasonics Symposium (IUS)* (IEEE, 2013), pp. 1501–1504.
- <sup>33</sup>A. H. Churchman, V. Mico, J. G. de Pablo, S. A. Peyman, S. Freear, and S. D. Evans, "Combined flow-focus and self-assembly routes for the formation of lipid stabilized oil-shelled microbubbles," *Microsyst. Nanoeng.* **4**(1), 17087 (2018).
- <sup>34</sup>V. Mico *et al.*, "Evaluation of lipid-stabilised tripropionin nanodroplets as a delivery route for combretastatin A4," *Int. J. Pharm.* **526**(1–2), 547–555 (2017).
- <sup>35</sup>A. Charalambous *et al.*, "Targeted microbubbles carrying lipid-oil-nanodroplets for ultrasound-triggered delivery of the hydrophobic drug, combretastatin A4," *Nanomed.: Nanotechnol., Biol. Med.* (published online) (2021).
- <sup>36</sup>N. Ingram *et al.*, "Ultrasound-triggered therapeutic microbubbles enhance the efficacy of cytotoxic drugs by increasing circulation and tumor drug accumulation and limiting bioavailability and toxicity in normal tissues," *Theranostics* **10**(24), 10973–10992 (2020).
- <sup>37</sup>M. D. Bourn *et al.*, "High-throughput microfluidics for evaluating microbubble enhanced delivery of cancer therapeutics in spheroid cultures," *J. Controlled Release* **326**, 13 (2020).
- <sup>38</sup>R. H. Abou-Saleh *et al.*, "Freeze-dried therapeutic microbubbles: Stability and gas exchange," *ACS Appl. Bio Mater.* **3**, 7840 (2020).
- <sup>39</sup>P. Bao, *et al.*, "Lipid coated liquid crystal droplets for the on-chip detection of antimicrobial peptides," *Lab Chip* **19**(6), 1082–1089 (2019).
- <sup>40</sup>S. A. Paymen, R. Hassan Abou-saleh, and S. D. Evans, "3D expanding geometry," U.S. patent US9802165B2 (31 October 2017).
- <sup>41</sup>D. V. B. Batchelor, MATLAB microbubble code, 2020.
- <sup>42</sup>R. H. Abou-Saleh *et al.*, "The influence of intercalating perfluoro-hexane into lipid shells on nano and microbubble stability," *Soft Matter* **12**(34), 7223–7230 (2016).
- <sup>43</sup>OPTISON™ (Perflutren Protein-Type A Microspheres Injectable Suspension, USP), GE Healthcare.
- <sup>44</sup>Vevo MicroMarker™ Non-Targeted Contrast Agent Kit: Booklet Contents: Micromarker Kit Content S, pp. 12–9.
- <sup>45</sup>ECHOVIST®, Canada, Berlex.
- <sup>46</sup>C. Hernandez *et al.*, "Sink or float? Characterization of shell-stabilized bulk nanobubbles using a resonant mass measurement technique," *Nanoscale* **11**(3), 851–855 (2019).
- <sup>47</sup>D. Midtvedt, F. Eklund, E. Olsén, B. Midtvedt, J. Swenson, and F. Höök, "Size and refractive index determination of subwavelength particles and air bubbles by holographic nanoparticle tracking analysis," *Anal. Chem.* **92**(2), 1908–1915 (2020).
- <sup>48</sup>A. J. Dixon, A. H. Dhanaliwala, J. L. Chen, and J. A. Hossack, "Enhanced intracellular delivery of a model drug using microbubbles produced by a microfluidic device," *Ultrasound Med. Biol.* **39**(7), 1267–1276 (2013).
- <sup>49</sup>T. Segers, D. Lohse, M. Versluis, and P. Frinking, "Universal equations for the coalescence probability and long-term size stability of phospholipid-coated monodisperse microbubbles formed by flow focusing," *Langmuir* **33**(39), 10329–10339 (2017).
- <sup>50</sup>P. Nittayacharn, H. X. Yuan, C. Hernandez, P. Bielecki, H. Zhou, and A. A. Exner, "Enhancing tumor drug distribution with ultrasound-triggered nanobubbles," *J. Pharm. Sci.* **108**, 3091–3098 (2019).